

# Boundary-Obstructed Topological Superfluids in Staggered Spin-Orbit Coupled Fermi Gases

Yu-Biao Wu,<sup>1</sup> Guang-Can Guo,<sup>1</sup> Zhen Zheng,<sup>2,\*</sup> and Xu-Bo Zou<sup>1,†</sup>

<sup>1</sup>*Key Laboratory of Quantum Information, and CAS Center for Excellence in Quantum Information and Quantum Physics, University of Science and Technology of China, Hefei, Anhui 230026, People's Republic of China*

<sup>2</sup>*Department of Physics and HKU-UCAS Joint Institute for Theoretical and Computational Physics at Hong Kong, The University of Hong Kong, Pokfulam Road, Hong Kong, China*

We present an experimental feasible proposal for synthesizing second-order topological superfluids that support Majorana corner modes in spin-orbit coupled Fermi gases. For this purpose, we consider the staggered spin-orbit coupling introduced in one direction. This results in a system consisted of two sublattices, providing extra degree of freedom for the emergent higher-order topological state. We find the topological trivial superfluids, first-order topological superfluids and boundary-obstructed second-order topological superfluids, as well as different topological phase transitions among them with respect to the the experimental tunable parameters. At the weak interaction regime, the phase transition is characterized by the Chern number accompanied by the bulk gap closing and reopening. However, at the strong interaction regime, we find the system can support the boundary-obstructed topological superfluids with Majorana corner modes, but topological phase transition dose not undergo the gap-closing of bulk bands. Instead the transition is refined by the quadrupole moment and signaled out by the gap-closing of edge-state. The proposal is simply based on the  $s$ -wave interaction and readily feasible via existing experimental techniques, which suggests new possibilities in interacting spin-orbit coupled systems by unifying both first- and higher-order topological superfluids in a simple but realistic microscopic model.

Compared with conventional solid-state systems, ultracold atoms in optical lattices offer a remarkable platform for investigating quantum many-body problems. Based on existing optical techniques, the high controllability and lack of disorder in ultracold atomic gases make it an ideal platform for the discovery of unconventional topological phases that are difficult to be realized or evidenced in ordinary condensed-matter systems [1, 2]. In particular, the engineering of the artificial gauge fields [3, 4] and nontrivial atomic interaction or pairing [5–11] facilitates the investigations in a variety of phenomena and phases, including the topological hall effect [12–17], topological insulators [18, 19], topological semimetals [20, 21], and topological superfluids [22–25]. Among them, the engineering topological superfluids has been attracted intensive interests for its unconventional non-Abelian exchange statistics and the potential application in fault-tolerant topological quantum computation [26].

It has been well known that traditional  $d$ -dimensional topological superfluids support a bulk gapped phases with topologically-protected Majorana edge modes (MEMs) on the  $d - 1$  dimensional boundaries [27], which is specified as a first-order topological superfluid (FOTSF) phase. By starkly contrast, for higher-order topological phases [28–34], both the  $d$ -dimensional bulk and the  $d - 1$  dimensional boundary are gapped, but the Majorana zero-energy modes (MZMs) arise at lower dimensions. Particularly, the boundary-obstructed topological phases, e.g. the second-order topological superfluids (SOTSF), support MZMs whose distribution are localized at corners of the two-dimensional (2D) lattice, i.e. the Majorana corner modes (MCMs) instead of MEMs.

A set of schemes in solids [35–44] have been proposed for realizing MCMs [35–38]. More recently, a novel class of the higher-order topological phases, which is also named as the boundary-obstructed topological phases [45] and characterized by gap-closing of edge states, attracts a great deal of attentions because of the enrichment of boundary physics. Several schemes have also been proposed for realizing the boundary-obstructed topological superconductivity [46, 47]. However, most of those schemes relies on nontrivial atomic interaction, which generally faces unexpected frustrations, such as the inelastic three-body scattering [48], to be implemented with current experimental technologies.

In this Letter, we aim to demonstrate an experimental feasible scheme for engineering the the boundary-obstructed topological superfluids, specifically SOTSF, in the ultracold Fermi gases. The main features of the proposal are as follows: (i) The system comprises an A-B sublattice structure, and the staggered spin-orbit (SO) coupling is required for realizing the boundary-obstructed topological phases. The engineering of the homogeneous SO coupling has been experimentally realized [49–53]. We extend these results and propose an experimental feasible scheme to realize the staggered SO coupling, which is used for the boundary-obstructed topological phases. (ii) The proposal is based on the conventional  $s$ -wave atomic interaction and overcomes practical frustrations in generating the unconventional atomic interaction. (iii) By changing the spatial modulation of the SO coupling, we find the first- and second-order topological transitions governed by different bulk-boundary correspondences. Especially during the second-order transi-

tion, the boundary-obstructed topological superfluids are distinguished not by gap-closings of the bulk bands but by those of the edge states.

*Model Hamiltonian and physical implementation.*— We start with the spinful Fermi gas trapped in a 2D optical lattice. The lattice model with a spatial periodicity of  $d$  is illustrated in FIG.1(a), which comprises an A-B sublattice structure. The Fermi gases can be described by the tight-binding model Hamiltonian composed of three parts,

$$H = H_0 + H_{\text{ext}} + H_{\text{int}}. \quad (1)$$

The first part describes the kinetic hopping term,

$$H_0 = - \sum_{j,s} \sum_{i=x,y} (t_i \psi_{j,s}^\dagger \psi_{j+\hat{e}_i,s} + H.c.) - \sum_{j,s} \mu \psi_{j,s}^\dagger \psi_{j,s}, \quad (2)$$

Here  $\psi_s$  denotes the field operator for fermionic atoms of pseudo-spin  $s = \uparrow, \downarrow$ .  $t_{x,y}$  is the magnitude of the nearest-neighbor (NN) hopping, and is chosen as the energy unit.  $\hat{e}_{x,y}$  stands for the unit vector.  $H.c.$  stands for the Hermitian conjugation.  $\mu$  is the chemical potential.

The second part of Hamiltonian (1) describes the external fields. To realize the boundary-obstructed topological superfluid phase, we consider the staggered Rashba-type SO coupling in accompany of a Zeeman field. Its form is given by

$$H_{\text{ext}} = \sum_{j,s,s'} V_z \psi_{j,s}^\dagger \sigma_z^{ss'} \psi_{j,s'} - (i\alpha_x \psi_{j,s}^\dagger \sigma_y^{ss'} \psi_{j+\hat{e}_x,s'} + H.c.) + [i\alpha_y (\psi_{2j-\hat{e}_y,s}^\dagger \sigma_x^{ss'} \psi_{2j,s'} + \eta \psi_{2j,s}^\dagger \sigma_x^{ss'} \psi_{2j+\hat{e}_y,s'}) + H.c.] \quad (3)$$

where  $\hat{\psi} \equiv (\psi_\uparrow, \psi_\downarrow)^T$ .  $\sigma_{x,y,z}$  are the Pauli matrices defined in the spin space.  $V_z$  is the strength of the Zeeman field.  $\alpha_{x,y}$  denotes the strength of the SO coupling. In general, an optical lattice can be dimerized in an A-B sublattice system via external optical fields [19, 21] or the manipulation of the lattice geometry [54–56]. In this way, it provides extra degrees of freedom that are presented by the sublattice index. Besides, the inter-sublattice interactions can be designed by the optical lattice configuration or laser fields. It paves the way to engineer interesting Hamiltonians in ultracold atoms. In this Letter, we follow this trick. Along the  $y$  direction, we modify the practical setup for generating  $t_y$  and  $\alpha_y$ . We impose a tilt gradient field  $\delta$  accompanied by a staggered offset  $\delta'$ , which are both spin independent as illustrated in FIG.1(b). The original NN hopping  $t_y$  is prohibited in presence of the gradient field  $\delta$ , however will be restored if we apply linear polarized optical fields  $G_1(\mathbf{r}) = G_1 \cos(2k_L y)$  and  $G_2(\mathbf{r}) = G_2 \cos(2k_L y)$  whose frequencies respectively compensate the detuning  $\delta \pm \delta'$  between atoms with the same spin in adjacent sites. Here  $k_L = \pi/d$ . In this setup, since the pseudo-spins stand for different atomic intrinsic hyperfine levels,

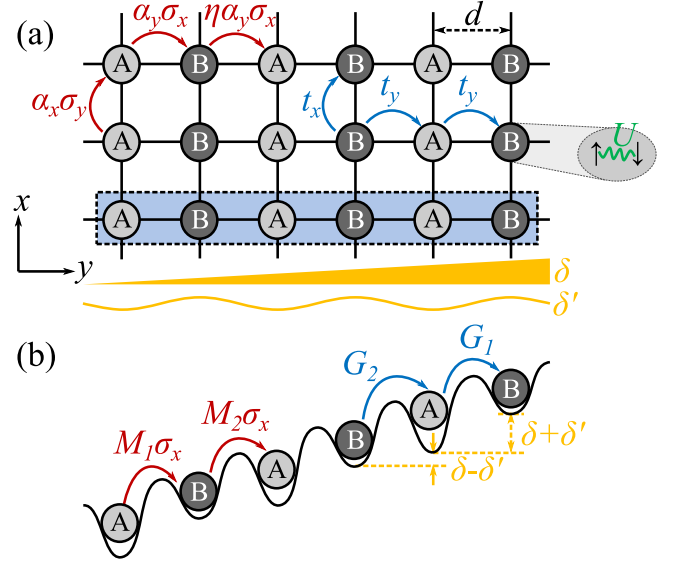


FIG. 1. (a) Illustration of the lattice model. The system is dimerized in A-B sublattices in presence of the staggered SO coupling  $\alpha_y$ . (b) Detailed setup for the blue dashed region in (a). The NN hopping  $t_y$  and staggered SO coupling  $\alpha_y$  are generated by the optical fields  $G_{1,2}$  and  $M_{1,2}$ , respectively.

the SO coupling  $\alpha_y$  can be instead engineered by the circular polarized optical fields  $M_1 = iM_1 \sin(k_L y)$  and  $M_2 = iM_2 \sin(k_L y)$ , whose frequencies also respectively compensate the detuning  $\delta \pm \delta'$ . The onsite spin hybridization is thus prohibited because of the odd parity of  $M_{1,2}(\mathbf{r})$  with respect to each site center. Meanwhile  $M_{1,2}(\mathbf{r})$  dose not lead to hopping between atoms with the same spin because this is forbidden by the selection rule. When the optical field strengths are prepared identical (i.e.  $G_1 = G_2$ ), the NN hopping is spatially uniform. But the SO coupling inherits a spatially staggered structure if the optical field strengths  $M_1 \neq M_2$ . One can find the spatial modulation of the SO coupling is characterized by the dimensionless parameter  $\eta = M_2/M_1$ , which is artificially tunable via the field strengths.

The last part of Hamiltonian (1) describes the  $s$ -wave interaction, which is usually controlled by Feshbach resonances,

$$H_{\text{int}} = - \sum_j U \psi_{j\uparrow}^\dagger \psi_{j\downarrow}^\dagger \psi_{j\downarrow} \psi_{j\uparrow}. \quad (4)$$

Here  $U$  denotes the interaction strength. The minus sign yields the interaction that we focus on is attractive. In cold atoms, this gives rise to the superfluid state, in which atoms form Cooper pairs in the same way as electrons do in superconductors of solids.

*Numerical results and phase diagram.*— In order to investigate nontrivial topological properties of the system, we employ the mean-field Bogoliubov-de Gennes (BdG) approach. By introducing the order parameters  $\Delta_j = -U \langle \psi_{j\downarrow} \psi_{j\uparrow} \rangle \approx \Delta$ , we can recast Hamiltonian (1)

into a matrix form, i.e. the BdG Hamiltonian. In particular, due to the presence of the staggered SO coupling, we rewrite Hamiltonian (1) in terms of A-B sublattices by invoking the following representation,

$$\psi_{2j-\hat{e}_y,s} \rightarrow a_{js}, \quad \psi_{2j,s} \rightarrow b_{js}. \quad (5)$$

In the transformation (5), the odd(even)-index sites along the  $y$  direction are mapped to the ones on A(B) sublattice, respectively.  $a$  and  $b$  are the corresponding atomic operators of the sublattices. In the momentum  $\mathbf{k}$  space, under the base  $\Psi = (a_{\mathbf{k},\uparrow}, b_{\mathbf{k},\uparrow}, a_{\mathbf{k},\downarrow}, b_{\mathbf{k},\downarrow}, a_{-\mathbf{k},\downarrow}^\dagger, b_{-\mathbf{k},\downarrow}^\dagger, -a_{-\mathbf{k},\uparrow}^\dagger, -b_{-\mathbf{k},\uparrow}^\dagger)^T$ , the BdG Hamiltonian is expressed as

$$\begin{aligned} H_{\text{BdG}}(\mathbf{k}) = & -[2t_x \cos(k_x d) + \mu]\tau_z - t_y[1 + \cos(k_y d)]\tau_z \zeta_x \\ & - t_y \sin(k_y d)\tau_z \zeta_y + V_z \sigma_z + \Delta \tau_x + 2\alpha_x \sin(k_x d)\tau_z \sigma_y \\ & + [\eta \alpha_y \cos(k_y d) - \alpha_y]\tau_z \sigma_x \zeta_y - \eta \alpha_y \sin(k_y d)\tau_z \sigma_x \zeta_x, \end{aligned} \quad (6)$$

Here  $\tau_{x,y,z}$  and  $\zeta_{x,y,z}$  are Pauli matrices defined on the particle-hole and  $a$ - $b$  operator basis.

For simplicity without loss of generality, in the following we shall choose  $t_x = t_y = t$  and  $\alpha_x = \alpha_y = \alpha$  to facilitate the further discussion. The order parameter  $\Delta$  can be obtained by self consistently minimizing the thermodynamic potential  $\Omega$ . At zero temperature,  $\Omega$  is given by

$$\Omega = \frac{1}{4} \sum_{\mathbf{k},\nu} E_\nu(\mathbf{k}) \Theta[-E_\nu(\mathbf{k})] + \mathcal{E}_0, \quad (7)$$

where  $E_\nu(\mathbf{k})$  is the energy of the  $\nu$ th eigenstate of Hamiltonian (6).  $\Theta(\cdot)$  is the Heaviside step function that is used to describe the Fermi-Dirac distribution at zero temperature. The energy constant  $\mathcal{E}_0 = |\Delta|^2/U + \sum_{\mathbf{k}} [-2t \cos(k_x d) - \mu - t - t \cos(k_y d)]$ . When  $\Delta \neq 0$ , it outlines the superfluid phase region, otherwise is a normal gas if  $\Delta$  vanishes.

We numerically obtain the order parameter  $\Delta$  by minimizing  $\Omega$ . The phase diagrams are displayed in FIG.2(a) and (b) with different interaction strengths. The superfluid phase region is composed of the trivial superfluid, FOTSF, and SOTSF phases. To distinguish the FOTSF and SOTSF phases, we inspect two topological invariants: the Chern number  $\mathcal{C}$  [58] and the quadrupole moment  $q_{xy}$  [31]. The Chern number is widely applied in characterizing MEMs, which is well known as bulk-edge correspondence. It is defined by

$$\mathcal{C} = \frac{1}{2\pi} \sum_n^{\text{occ.}} \int F_{nz} d\mathbf{k} \quad (8)$$

with Berry curvature defined as  $\mathbf{F}_n = \nabla \times \mathbf{A}_n$  and Berry connection  $\mathbf{A}_n = -i \langle u_{n\mathbf{k}} | \frac{\partial}{\partial \mathbf{k}} | u_{n\mathbf{k}} \rangle$ . The summation  $\sum_n^{\text{occ.}}$  takes over all the occupied quasi-particle bands and  $|u_{n\mathbf{k}}\rangle$  is the  $n$ th occupied eigenstate. The

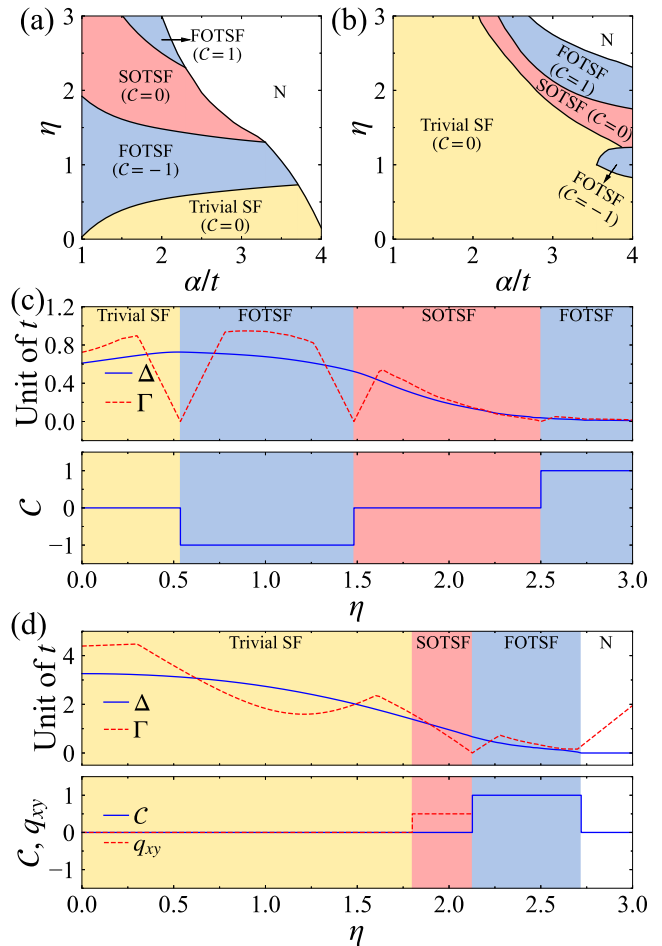


FIG. 2. (a)-(b) Phase diagrams at (a)  $U = 6t$  and (b)  $U = 12t$ . Other parameters are  $\mu = 3t$  and  $V_z = 2t$ . Trivial SF and N stand for the trivial superfluid and normal gas phase, respectively. (c)-(d) The order parameter  $\Delta$ , bulk gap  $\Gamma$ , and Chern number  $\mathcal{C}$  as functions of  $\eta$  at (c)  $(U, \alpha) = (6t, 2t)$  and (d)  $(12t, 3t)$ . In (d), the quadrupole moment  $q_{xy}$  is available for the trivial superfluid and SOTSF phases [57].

quadrupole moment can be calculated by means of the nested Wilson loop formalism [59]. It refines the topologically protected charges that characterizes the existence of MCMs. In particular, the quadrupole moment is defined by [31] as

$$q_{xy} = p_y^{\nu_x^+} p_x^{\nu_y^+} + p_y^{\nu_x^-} p_x^{\nu_y^-}, \quad (9)$$

where the invariants  $p_y^{\nu_x^\pm}$  and  $p_x^{\nu_y^\pm}$  are calculated by the Wannier sector polarizations [60]. The system lies in SOTSF when  $q_{xy}$  is half quantized, otherwise is topologically trivial when  $q_{xy}$  vanishes.

The phase diagram exhibits distinct behaviors at different regimes in terms of the interaction strength  $U$ . At weak interaction limit, c.f. FIG.2(a), we find two FOTSF regions with Chern numbers of opposite signs. Specifically, when  $\eta = 1$ , Hamiltonian (1) is reduced to the stan-

standard model and well known for supporting MEMs [22]. The SOTSF phase with a zero Chern number is isolated from the trivial superfluid phase by the FOTSF regions. At strong interaction limit shown in FIG.2(b), besides the transition between two different topological phases, one can find the system can undergo a direct transition from the trivial superfluid phase to the SOTSF one. The Chern number remains zero and thereby inadequate to figure out the phase transition.

We emphasize that the crucial feature of the existed topological transitions relies on the intrinsic bulk-boundary correspondence, but in various ways. To extract the underlying properties of topological transition, we firstly plot the bulk gap  $\Gamma$  and the Chern number  $\mathcal{C}$  with respect to  $\eta$  in FIG.2(c) and (d). At weak interaction regime, the bulk gap closes and reopens at the transition between different topological phases, as shown in FIG.2(c). This is consistent to the conventional physics picture, in which the topological transition occurs in accompany of the bulk gap closing as well as the changed Chern number. The topological transition is known of the first order, and obeys the ubiquitous bulk-edge correspondence. The existed edge states are topologically protected in FOTSF unless the bulk gap closes. However, at strong interaction regime, an exotic topological transition without gap closing processes from the trivial superfluid to SOTSF phases, during which the quadrupole moment  $q_{xy}$  plays the role of the topological invariant as shown in FIG.2(d). In order to capture the features of the SOTSF transition, we use the cylindrical geometry by imposing a periodic boundary condition in the  $x$  direction. The quasi-particle spectrum  $E_\nu$  is obtained by diagonalizing the BdG Hamiltonian in spatial space, shown in FIG.3(a)-(c). In the trivial phase, the system hosts gapped edge states that are not topological protected. By increasing  $\eta$ , the edge-state gap closes at the critical point and reopens when system evolves into the SOTSF phase. Therefore, the topological transition without bulk closing is of the second order, signaled by the edge-state gap. The second-order topological transition follows the edge-corner correspondence [61] rather than the bulk-edge correspondence. In another words, the corners of the lattice plaquette play the role of boundaries while the edges are regarded as the bulk. SOTSF supports the MCMs with zero energy whose density distributions are fully localized in the four corners, as shown in FIG.3(d). The MCMs does not vanish without closing the edge-state gap.

The Hamiltonian (6) of system obviously preserves the particle-hole symmetry:  $\mathcal{P}H_{\text{BdG}}(\mathbf{k})\mathcal{P}^{-1} = -H_{\text{BdG}}(-\mathbf{k})$  with  $\mathcal{P} = \tau_y\sigma_y\mathcal{K}$  and  $\mathcal{K}$  standing for the complex conjugation. In presence of the Zeeman field  $V_z$ , the time-reversal symmetry is broken. Moreover, the system does not have chiral symmetry because Hamiltonian (6) is not invariant by exchanging the  $a$  and  $b$  operators. Therefore, the edge states are two-fold degenerate, resulting in

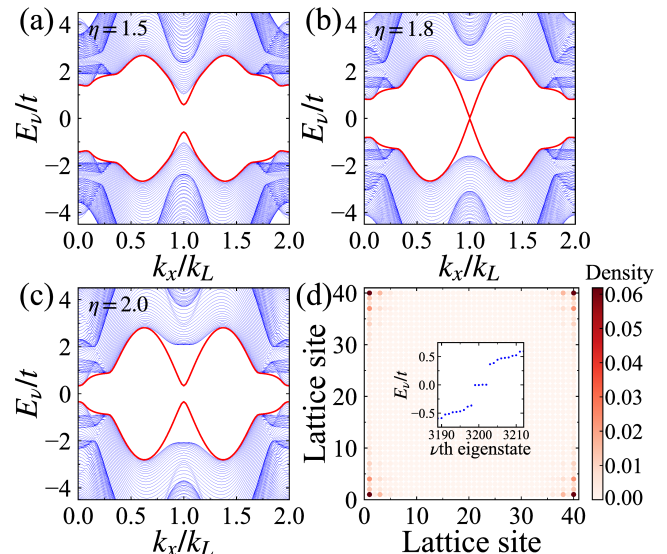


FIG. 3. (a)-(c) The quasi-particle spectrum with cylindrical geometry for different  $\eta$  at  $(U, \alpha) = (12t, 3t)$ . Other parameters are the same with FIG.2(b). The two-fold degenerate edge-state spectrum is highlighted by red solid lines. (d) The spatial distribution of the MCMs in (c). The colors characterize the density magnitudes. The inset shows the quasi-particle spectrum in the vicinity of zero energy. We employ the open boundary condition in both the  $x$  and  $y$  directions. The lattice size is set as  $L \times L$  with  $L = 40$ .

four-fold MCMs as shown in FIG.3(d).

*Discussions and Conclusion.*— In practice, the tilt gradient field  $\delta$  is commonly introduced via a magnetic gradient, which is widely applied in the laser-assisted tunneling technique [62, 63]. For the staggered offset  $\delta'$ , we can engineer a spatial periodic Stark shift to atoms, whose periodicity is two times of the lattice one, c.f. FIG.1(a). We remark that the choose of the spatial modulation of  $G_{1,2}(\mathbf{r})$  and  $M_{1,2}(\mathbf{r})$  is necessary. This is because, in the Wannier picture of the tight-binding model, the atomic wave functions in adjacent sites are orthogonal, hence no hopping or coupling is generated if one use spatially uniform fields instead. Along the  $y$  direction,  $M_{1,2}(\mathbf{r})$  is of the odd parity with respect to each site center. Thus the engineered coupling between adjacent sites will have an opposite sign in terms of the hopping direction, exhibiting the prominent property of the SO coupling.

In summary, we demonstrate an experimental feasible scheme for engineering the the boundary-obstructed second-order topological superfluids that supports MCMs. The staggered SO coupling leads to the topological phase transition, yet exhibiting distinct phenomena by changing the  $s$ -wave interaction. The FOTSF and SOTSF phase transitions are separately characterized by different topological invariants as well as band gap signals, revealing various bulk-boundary correspondences. The proposal is feasible by means of current experimen-

tal techniques, and can pave the way for exploring the boundary-obstructed phases and the associated MCMs.

*Acknowledgements.*— This work is supported by National Natural Science Foundation of China (Grants No. 11474271, 11674305, and 11704367).

---

\* zhenzhen.dr@outlook.com

† xbz@ustc.edu.cn

- [1] I. Bloch, J. Dalibard, and S. Nascimbène, *Nat. Phys.* **8**, 267 (2012).
- [2] C. Gross and I. Bloch, *Science* **357**, 995 (2017).
- [3] N. Goldman, G. Juzeliūnas, P. Öhberg, and I. B. Spielman, *Rep. Prog. Phys.* **77**, 126401 (2014).
- [4] A. Eckardt, *Rev. Mod. Phys.* **89**, 011004 (2017).
- [5] C. A. Regal, C. Ticknor, J. L. Bohn, and D. S. Jin, *Phys. Rev. Lett.* **90**, 053201 (2003).
- [6] K. A. Kuns, A. M. Rey, and A. V. Gorshkov, *Phys. Rev. A* **84**, 063639 (2011).
- [7] C. V. Kraus, M. Dalmonte, M. A. Baranov, A. M. Läuchli, and P. Zoller, *Phys. Rev. Lett.* **111**, 173004 (2013).
- [8] B. Liu, X. Li, L. Yin, and W. V. Liu, *Phys. Rev. Lett.* **114**, 045302 (2015).
- [9] S.-L. Zhang, L.-J. Lang, and Q. Zhou, *Phys. Rev. Lett.* **115**, 225301 (2015).
- [10] Y. Cui, C. Shen, M. Deng, S. Dong, C. Chen, R. Lü, B. Gao, M. K. Tey, and L. You, *Phys. Rev. Lett.* **119**, 203402 (2017).
- [11] X.-C. Yao, R. Qi, X.-P. Liu, X.-Q. Wang, Y.-X. Wang, Y.-P. Wu, H.-Z. Chen, P. Zhang, H. Zhai, Y.-A. Chen, and J.-W. Pan, *Nat. Phys.* **15**, 570 (2019).
- [12] R. N. Palmer, A. Klein, and D. Jaksch, *Phys. Rev. A* **78**, 013609 (2008).
- [13] M. Aidelsburger, M. Atala, S. Nascimbène, S. Trotzky, Y.-A. Chen, and I. Bloch, *Phys. Rev. Lett.* **107**, 255301 (2011).
- [14] A. Celi, P. Massignan, J. Ruseckas, N. Goldman, I. B. Spielman, G. Juzeliūnas, and M. Lewenstein, *Phys. Rev. Lett.* **112**, 043001 (2014).
- [15] B. K. Stuhl, H.-I. Lu, L. M. Ayccock, D. Genkina, and I. B. Spielman, *Science* **349**, 1514 (2015).
- [16] T. Graß, C. Muschik, A. Celi, R. W. Chhajlany, and M. Lewenstein, *Phys. Rev. A* **91**, 063612 (2015).
- [17] C. Kollath, A. Sheikhan, S. Wolff, and F. Brennecke, *Phys. Rev. Lett.* **116**, 060401 (2016).
- [18] T. D. Stanescu, V. Galitski, J. Y. Vaishnav, C. W. Clark, and S. Das Sarma, *Phys. Rev. A* **79**, 053639 (2009).
- [19] C. J. Kennedy, G. A. Siviloglou, H. Miyake, W. C. Burton, and W. Ketterle, *Phys. Rev. Lett.* **111**, 225301 (2013).
- [20] K. Sun, W. V. Liu, A. Hemmerich, and S. Das Sarma, *Nat. Phys.* **8**, 67 (2011).
- [21] T. Dubček, C. J. Kennedy, L. Lu, W. Ketterle, M. Soljačić, and H. Buljan, *Phys. Rev. Lett.* **114**, 225301 (2015).
- [22] M. Gong, S. Tewari, and C. Zhang, *Phys. Rev. Lett.* **107**, 195303 (2011).
- [23] C. Qu, Z. Zheng, M. Gong, Y. Xu, L. Mao, X. Zou, G. Guo, and C. Zhang, *Nat. Commun.* **4**, 2710 (2013).
- [24] W. Zhang and W. Yi, *Nat. Commun.* **4**, 2711 (2013).
- [25] C. Chan, L. Zhang, T. F. J. Poon, Y.-P. He, Y.-Q. Wang, and X.-J. Liu, *Phys. Rev. Lett.* **119**, 047001 (2017).
- [26] C. Nayak, S. H. Simon, A. Stern, M. Freedman, and S. Das Sarma, *Rev. Mod. Phys.* **80**, 1083 (2008).
- [27] M. Z. Hasan and C. L. Kane, *Rev. Mod. Phys.* **82**, 3045 (2010).
- [28] F. Schindler, A. M. Cook, M. G. Vergniory, Z. Wang, S. S. P. Parkin, B. A. Bernevig, and T. Neupert, *Sci. Adv.* **4**, eaat0346 (2018).
- [29] F. Zhang, C. L. Kane, and E. J. Mele, *Phys. Rev. Lett.* **110**, 046404 (2013).
- [30] W. A. Benalcazar, J. C. Y. Teo, and T. L. Hughes, *Phys. Rev. B* **89**, 224503 (2014).
- [31] W. A. Benalcazar, B. A. Bernevig, and T. L. Hughes, *Science* **357**, 61 (2017).
- [32] W. A. Benalcazar, B. A. Bernevig, and T. L. Hughes, *Phys. Rev. B* **96**, 245115 (2017).
- [33] J. Langbehn, Y. Peng, L. Trifunovic, F. von Oppen, and P. W. Brouwer, *Phys. Rev. Lett.* **119**, 246401 (2017).
- [34] Y. Peng, Y. Bao, and F. von Oppen, *Phys. Rev. B* **95**, 235143 (2017).
- [35] Z. Yan, F. Song, and Z. Wang, *Phys. Rev. Lett.* **121**, 096803 (2018).
- [36] T. Liu, J. J. He, and F. Nori, *Phys. Rev. B* **98**, 245413 (2018).
- [37] M. Ezawa, *Phys. Rev. Lett.* **121**, 116801 (2018).
- [38] X. Zhu, *Phys. Rev. B* **97**, 205134 (2018).
- [39] X. Zhu, *Phys. Rev. Lett.* **122**, 236401 (2019).
- [40] M. Ezawa, *Phys. Rev. B* **97**, 155305 (2018).
- [41] Y. Volpez, D. Loss, and J. Klinovaja, *Phys. Rev. Lett.* **122**, 126402 (2019).
- [42] Y.-J. Wu, J. Hou, Y.-M. Li, X.-W. Luo, X. Shi, and C. Zhang, *Phys. Rev. Lett.* **124**, 227001 (2020).
- [43] M. Kheirkhah, Z. Yan, Y. Nagai, and F. Marsiglio, *Phys. Rev. Lett.* **125**, 017001 (2020).
- [44] Y.-B. Wu, G.-C. Guo, Z. Zheng, and X.-B. Zou, *Phys. Rev. A* **101**, 013622 (2020).
- [45] E. Khalaf, W. A. Benalcazar, T. L. Hughes, and R. Queiroz, (2019), [arXiv:1908.00011](https://arxiv.org/abs/1908.00011).
- [46] X. Wu, W. A. Benalcazar, Y. Li, R. Thomale, C.-X. Liu, and J. Hu, (2020), [arXiv:2003.12204](https://arxiv.org/abs/2003.12204).
- [47] A. Tiwari, A. Jahin, and Y. Wang, (2020), [arXiv:2005.12291](https://arxiv.org/abs/2005.12291).
- [48] J. Levinsen, N. R. Cooper, and V. Gurarie, *Phys. Rev. A* **78**, 063616 (2008).
- [49] Y.-J. Lin, K. Jiménez-García, and I. B. Spielman, *Nature* **471**, 83 (2011).
- [50] S. Kolkowitz, S. L. Bromley, T. Bothwell, M. L. Wall, G. E. Marti, A. P. Koller, X. Zhang, A. M. Rey, and J. Ye, *Nature* **542**, 66 (2016).
- [51] L. Huang, Z. Meng, P. Wang, P. Peng, S.-L. Zhang, L. Chen, D. Li, Q. Zhou, and J. Zhang, *Nat. Phys.* **12**, 540 (2016).
- [52] Z. Wu, L. Zhang, W. Sun, X.-T. Xu, B.-Z. Wang, S.-C. Ji, Y. Deng, S. Chen, X.-J. Liu, and J.-W. Pan, *Science* **354**, 83 (2016).
- [53] C. Hammer, C. Qu, Y. Zhang, J. Chang, M. Gong, C. Zhang, and P. Engels, *Nat. Commun.* **5**, 4023 (2014).
- [54] L. Tarruell, D. Greif, T. Uehlinger, G. Jotzu, and T. Esslinger, *Nature* **483**, 302 (2012).
- [55] G. Jotzu, M. Messer, R. Desbuquois, M. Lebrat, T. Uehlinger, D. Greif, and T. Esslinger, *Nature* **515**, 237 (2014).
- [56] F. Görg, M. Messer, K. Sandholzer, G. Jotzu, R. Des-

- buquois, and T. Esslinger, *Nature* **553**, 481 (2018).
- [57]  $q_{xy}$  is not available for FOTSF because the Wannier sectors used in the calculation of  $q_{xy}$  are gapless over the entire Brillouin zone. But the transition from FOTSF to other phases can still be signaled by the Chern number.
- [58] T. Fukui, Y. Hatsugai, and H. Suzuki, *J. Phys. Soc. Jpn.* **74**, 1674 (2005).
- [59] S. Franca, J. van den Brink, and I. C. Fulga, *Phys. Rev. B* **98**, 201114 (2018).
- [60] See the Supplemental Materials.
- [61] M. Ezawa, (2020), [arXiv:2007.03884](https://arxiv.org/abs/2007.03884).
- [62] M. Aidelsburger, M. Atala, M. Lohse, J. T. Barreiro, B. Paredes, and I. Bloch, *Phys. Rev. Lett.* **111**, 185301 (2013).
- [63] H. Miyake, G. A. Siviloglou, C. J. Kennedy, W. C. Burton, and W. Ketterle, *Phys. Rev. Lett.* **111**, 185302 (2013).

## Supplemental Materials

Here we present the technical details in calculating the quadrupole momentum by means of the Nested Wilson loops. We firstly diagonalize the total 8-band Hamiltonian and obtain the  $N_{\text{occ}} = 4$  occupied states  $|u_{\mathbf{k}}^m\rangle$ . Then we define the Wilson loop operators  $\mathcal{W}_{x,\mathbf{k}}$  and  $\mathcal{W}_{y,\mathbf{k}}$  in the  $x$  and  $y$  directions, where  $\mathbf{k} = (k_x, k_y)$  is the initial point of the Wilson loop operator. For the  $L \times L$  square lattice, by using the obtained occupied states, we define  $N_{\text{occ}} \times N_{\text{occ}}$ -dimension matrix  $[G_{x,\mathbf{k}}]^{mn} = \langle u_{\mathbf{k}+\Delta\mathbf{k}_x}^m | u_{\mathbf{k}}^n \rangle$ , where  $\Delta\mathbf{k}_{x,y} = \frac{2\pi}{L}\hat{\mathbf{e}}_{x,y}$ . Thus we can define the Wilson loop operator in the discrete limit

$$W_{x,\mathbf{k}} = G_{x,\mathbf{k}+L\Delta\mathbf{k}_x} \cdots G_{x,\mathbf{k}+\Delta\mathbf{k}_x} G_{x,\mathbf{k}}. \quad (\text{S1})$$

Because of the discretization of momentum  $\mathbf{k}$ , the matrix  $G$  is not a unitary matrix. It can be mapped to be unitary by the singular value decomposition (SVD) at each discretized momentum:  $G_{x,\mathbf{k}} = UDV^\dagger$ . In this way, by redefining  $F_{x,\mathbf{k}} = UV^\dagger$ , we can rewrite the unitary Wilson loop operator as

$$\mathcal{W}_{x,\mathbf{k}} = F_{x,\mathbf{k}+L\Delta\mathbf{k}_x} \cdots F_{x,\mathbf{k}+\Delta\mathbf{k}_x} F_{x,\mathbf{k}}. \quad (\text{S2})$$

Under the periodic boundary condition of a torus geometry, the eigenequation of the Wilson loop operator is expressed as

$$\mathcal{W}_{x,\mathbf{k}} |\nu_{x,\mathbf{k}}^{\pm,r}\rangle = e^{2\pi i v_x^j(k_y)} |\nu_{x,\mathbf{k}}^{\pm,r}\rangle. \quad (\text{S3})$$

Here  $\pm$  represent two different Wannier sectors, and  $r = 1 \dots N_{\text{occ}}/2$ . The nested Wilson loops along  $y$ -direction is thus obtained as

$$\tilde{\mathcal{W}}_{y,\mathbf{k}_x}^{\pm} = F_{y,\mathbf{k}+L\Delta\mathbf{k}_y}^{\pm} \cdots F_{y,\mathbf{k}+\Delta\mathbf{k}_y}^{\pm} F_{y,\mathbf{k}}^{\pm}, \quad (\text{S4})$$

where

$$F_{y,\mathbf{k}}^{\pm} = \langle w_{x,\mathbf{k}+\Delta\mathbf{k}_y}^{\pm,r} | w_{x,\mathbf{k}}^{\pm,r} \rangle, \quad |w_{x,\mathbf{k}}^{\pm,r}\rangle = \sum_{n=1}^{N_{\text{occ}}} |u_{\mathbf{k}}^n\rangle [\nu_{x,\mathbf{k}}^{\pm,r}]^n. \quad (\text{S5})$$

$[\nu_{x,\mathbf{k}}^{\pm,r}]^n$  are the components of the Wilson loop eigenstate  $|\nu_{x,\mathbf{k}}^{\pm,r}\rangle$ . The Wannier sector polarization is given by

$$p_y^{\nu_x^{\pm}} = -\frac{i}{2\pi} \frac{1}{L} \sum_{k_x} \text{Log}[\tilde{\mathcal{W}}_{y,\mathbf{k}_x}^{\pm}], \quad (\text{S6})$$

It is specified as a  $\mathbb{Z}_2$  topological index:  $p_y^{\nu_x^{\pm}} \in \{0, 1/2\}$ . Likewise, the other topological index  $p_x^{\nu_y^{\pm}}$  can be obtained following the same approach.

The quadrupole invariant  $q_{xy}$  is expressed as

$$q_{xy} = p_y^{\nu_x^+} p_x^{\nu_y^+} + p_y^{\nu_x^-} p_x^{\nu_y^-}. \quad (\text{S7})$$

In the SOTSF phase with  $(p_x^{\nu_y^{\pm}}, p_y^{\nu_x^{\pm}}) = (1/2, 1/2)$ , we have a half quantized quadrupole moment  $q_{xy}$ . In otherwise phases with  $(p_x^{\nu_y^{\pm}}, p_y^{\nu_x^{\pm}}) = (1/2, 0)$  or  $(0, 0)$ ,  $q_{xy}$  vanishes. Therefore,  $q_{xy}$  can play the role of a topological invariant featuring in the transition between the trivial superfluid and SOTSF phases.

We note that  $q_{xy}$  is not available for FOTSF because the two Wannier sectors are gapless over the entire Brillouin zone. But the transition from FOTSF to other phases can still be characterized by the Chern number as in the conventional physics picture.